

Estimates of relativistic electron and proton energy densities in starburst galactic nuclei from radio measurements

Massimo Persic^{1,2} and Yoel Rephaeli^{3,4}

¹ INAF-Trieste, via G.B. Tiepolo 11, I-34143 Trieste, Italy

² INFN-Trieste, via A. Valerio 2, I-34127 Trieste, Italy

³ School of Physics & Astronomy, Tel-Aviv University, Tel Aviv 69978, Israel

⁴ Center for Astrophysics & Space Sciences, University of California at San Diego, La Jolla, CA 92093, USA

Received; accepted

Abstract. The energy density of energetic protons, U_p , in several nearby starburst nuclei (SBN) has been directly deduced from γ -ray measurements of the radiative decay of π^0 produced in interactions with ambient protons. Lack of sufficient sensitivity and spatial resolution makes this direct deduction unrealistic in the foreseeable future for (even) a moderately distant SBN. A more viable indirect method to determine U_p in star-forming galaxies is to use its theoretically-based scaling to the energy density of energetic electrons, U_e , which can be directly deduced from radio synchrotron and possibly also nonthermal hard X-ray emission. In order to improve the quantitative basis and diagnostic power of this leptonic method we re-formulate and clarify its main aspects. Doing so we obtain a basic expression for the ratio U_p/U_e in terms of the proton and electron masses and the power-law indices that characterize the particle spectral distributions in regions where the (total) particle energy density is at equipartition with that of the mean magnetic field. We also express the field strength and the particle energy density in the equipartition region in terms of the region's size, mean gas density, IR and radio fluxes, and distance, and determine values of U_p in a sample of 9 nearby SBNs.

Key words. diffuse radiation – galaxies: starburst – galaxies: radio emission – cosmic rays: observations – galaxies: individual

1. Introduction

Supernovae (SN) are thought to be the main drivers of particle acceleration via the Fermi-I diffusive shock mechanism (e.g., Gaisser 1990). The radiative yields of relativistic electrons and protons have been measured in the radio to TeV regions.

Proton interactions with ambient gas protons produce neutral pions (π^0), whose decay into γ -rays is the most significant signature of the main component of cosmic rays (CRs). Measurement of this emission yields the key ingredient in the energetics of galactic nonthermal particles, and together with synchrotron and Compton emissions by RE, allows relating diverse phenomena such as star formation (SF) and SN rates, efficiency of particle acceleration, and magnetic fields strength. The high SF rates and dense gas in starburst nuclei (SBN) make these regions prime targets for exploring this relation between stellar and nonthermal quantities to explore these environments.

In a SBN with H-nuclei number density n and volume V , the integrated hadronic γ -ray emission from π^0 decay is

$$L_{\geq \epsilon}^{[q_p]} \sim \int_V g_{\geq \epsilon}^{[q_p]} n U_p dV \quad \text{s}^{-1} \quad (1)$$

with the integral emissivity $g_{\geq \epsilon}^{[q_p]}$ measured in units of $\text{photon s}^{-1}(\text{H-atom})^{-1}(\text{eV/cm}^3)^{-1}$, and q_p is the spectral index of the proton power-law distribution (Drury et al. 1994). U_p can be determined from the measured value of $L_{\geq \epsilon}^{[q_p]}$ if $n(r)$ is known. In steady-state the spectro-spatial particle distributions can be calculated by numerically solving a convection-diffusion equation which includes all the relevant energy losses (e.g., Paglione et al. 1996; Torres 2004). Normalizing the particle distributions based on their measured radiative yields estimates of their energy densities. In particular, measurement of the π^0 -decay γ -ray emission is essentially the most direct way to determine U_p .

Improving the physical basis for a reliable extraction of the proton energy density, U_p , from γ -ray measurements is well motivated and timely, in light of recent satellite and ground-based observations. These include the detection of three nearby starburst galaxies, NGC 253, NGC 3034 (M 82), and NGC 5945, in the GeV (Ackermann et al. 2012) and TeV (Acero et al. 2009; Acciari et al. 2009; Lenain et al. 2010) regions. Measured fluxes from these galaxies are in accord with earlier theoretical predictions (NGC 253: Domingo-Santamaría & Torres 2005, Rephaeli et al. 2010; NGC 3034: Persic et al. 2008, de Cea et al. 2009; NGC 4945: Lenain et al. 2010) based on convection-diffusion models for proton and electron prop-

agation and energy losses. While there were appreciable differences in the models treated in those works, predicted values for U_p in the SB nuclei of the three galaxies were around 250 eV cm^{-3} .

Even though most of the energetic particle energy is in protons, the level of the unbeamed hadronic emission in most SBN is not sufficiently high for obtaining a reliable estimation of U_p from the measurement of hadronic γ -ray emission. This is the main reason for the fact that, with current detector sensitivities, γ -ray emission was detected (as we just noted) in only three nearby SBGs. It is therefore quite important to re-formulate the ‘leptonic’ route for estimating particle energy densities, testing its viability in the these three SBGs, and applying the insight gained from applications of both methods to these nearby galaxies to improve the precision with which U_p and U_e can be determined in SBGs.

Starting with estimates of the duration of a SB phase, acceleration, energy loss and advection relevant timescales, we show that particle distributions can be in steady state in a SBN. We continue with the usual assumptions in order to relate the proton and electron densities by charge neutrality, and energy densities through equipartition with the mean magnetic field. Doing so we re-formulate the hadronic and leptonic methods for determining particle energy densities from measurements of radio and γ -ray emission, and refine the expressions for the proton-to-electron density and energy density ratios. We then obtain an expression for the equipartition magnetic field and particle energy densities in a SBN in terms of assumed (theoretically-based) value of the spectral index of the proton density, and basic measured parameters characterizing the region – size, gas density, IR luminosity, radio flux, radio spectral index, and distance.

In Section 2 we assess the viability of the standard assumption that particle distributions attain a steady-state, and the likelihood of reaching energy equipartition with the mean magnetic field in the SBN. The basic expressions for p/e ratios and for U_p in terms of the electron synchrotron flux are written in Sect. 3. In Section 4 these expressions are applied to a sample of nearby and local SBN. We conclude with a discussion and a summary in Sect. 5.

2. Energy loss and propagation timescales

The benchmark timescale for enhanced stellar activity in a SBN – the duration of the SB phase – is typically estimated to be $t_{\text{SB}} \sim 10^8 \text{ yr}$. This characteristic time sets the scale for the assessment of temporal non-variability of particle distributions. Specifically, particle densities may attain a steady state if their characteristic acceleration and the weighted energy loss (by collisions and through propagation out of the SBN) timescales are considerably shorter than t_{SB} . If so, and the acceleration and energy loss timescales are comparable, the particle (spectral) densities are in a steady state.

Acceleration in a SN remnant (SNR) by the Fermi-I process occurs on a timescale $t_{\text{acc}} \equiv E/\dot{E} = (\Delta E/E)^{-1} \Delta t = \beta^{-1} \Delta t = (30/\beta_{0.033}) \Delta t \sim 3 \times 10^5 \text{ yr}$, where $\Delta t \sim 10^4 \text{ yr}$ is a typical SNR lifetime, and $\beta_{0.033}$ is the speed of the SN shock

in units of $0.033 c = 10^4 \text{ km s}^{-1}$. Clearly, particle acceleration to all relevant energies occurs on a relatively short timescale.

Protons lose energy mainly by pp interactions and escape out of the SBN, on a characteristic timescale $t_p^{-1} = t_{\text{pp}}^{-1} + t_{\text{out}}^{-1}$. The latter are the energy-loss timescales for pp interactions, $t_{\text{pp}} = (\sigma_{\text{pp}} c n)^{-1}$ (with σ_{pp} denoting the corresponding total cross section), and for particle removal, $t_{\text{out}}^{-1} = t_{\text{adv}}^{-1} + t_{\text{diff}}^{-1}$, where t_{adv} is the timescale for advection in a large-scale outflow (i.e., a galactic wind) and t_{diff} is the diffusion time. In the energy range $10 - 10^5 \text{ GeV}$, $\sigma_{\text{pp}} \sim 50 \text{ mb}$, so that $t_{\text{pp}} \sim 2 \times 10^5 \left(\frac{n}{100 \text{ cm}^{-3}} \right)^{-1} \text{ yr}$. For a homogeneous distribution of SN in a SBN of radius r_s , the advection timescale for transfer of particles out of the disk mid-plane region in a fast ($v_{\text{adv}} \sim 1000 \text{ km s}^{-1}$) SB-driven wind¹ is $t_{\text{adv}} = 5 \times 10^4 (r_s/0.2 \text{ kpc}) (v_{\text{out}}/1000 \text{ km s}^{-1})^{-1} \text{ yr}$. Particle diffusion is likely to be dominated by random-walk through the tangled magnetic fields in the SBN. In this dense region the field coherence scale is expected to be much smaller than in the disk (where the small-scale cellular structure has a coherence scale $\sim 100 \text{ pc}$), so scaling to a value of 3 pc , the characteristic diffusion time of protons in the SBN is $t_{\text{diff}} = 1.3 \times 10^5 (r_s/0.2 \text{ kpc})^2 (\lambda/3 \text{ pc})^{-1} \text{ yr}$ – a value comparable to t_{adv} . From $t_p^{-1} = t_{\text{pp}}^{-1} + t_{\text{out}}^{-1}$, we get $t_p \sim 3 \times 10^4 \text{ yr}$ for fiducial parameter values typical for SBN.

The electron energy loss timescale is determined by Coulomb, bremsstrahlung, synchrotron & Compton processes, and escape out of the SBN, $t_e^{-1} = t_C^{-1} + t_{\text{br}}^{-1} + t_{\text{SC}}^{-1} + t_{\text{out}}^{-1}$, respectively. Limiting the discussion here to electron energies higher than a threshold value γ_1 below which Coulomb losses become relevant (see Sect. 4), we can ignore this non-radiative process in the estimation of the weighted mean energy loss time. The bremsstrahlung cooling time for electrons traveling through ionized gas with number density n is $t_{\text{br}} = 4.4 \times 10^7 n^{-1} \text{ yr}$. The synchrotron-Compton time for electrons traversing a region with disordered magnetic field B with energy density $U_B = B^2/(8\pi)$, and IR energy density $U_{\text{IR}} = L_{\text{IR}}/(4\pi r^2 c)$, is $t_{\text{SC}} = \frac{3m_e c}{4\sigma_T} \gamma^{-1} (U_B + U_{\text{ph}})^{-1} \simeq \gamma^{-1} (U_B + U_{\text{ph}})^{-1} \text{ yr}$. Under typical conditions in SBN (which are fully specified in Sect. 4; see also Fig. 1) the weighted energy loss time for high energy electrons is $t_e \sim 4.3 \times 10^4 \text{ yr}$ for $\gamma \sim 10^3$.

Since typical acceleration and energy loss times are much shorter than the SB duration, particle spectral densities can attain steady state at levels that are proportional to the respective ratio of the energy loss time to the acceleration time. More generally, in a state of hydrostatic and virial equilibrium, it is likely that in the minimum energy configuration energy densities of particles and magnetic fields, which are tightly coupled dynamically and energetically in the SN environment, are in energy equipartition (e.g., Longair 1981). Generally, the denser and more radiatively intense the environment, the tighter is the coupling between all degrees of freedom, including nonthermal particles and magnetic fields. Physical processes that couple between nonthermal particles and thermal

¹ This velocity seems appropriate for NGC 3034, given the terminal outflow velocity of $1600 - 2200 \text{ km s}^{-1}$ deduced by Strickland & Heckman (2009; see also Chevalier & Clegg 1985).

gas are Coulomb interactions (i.e., ionization, electronic excitations, and bremsstrahlung), Compton scattering, and excitation of magnetic turbulence (e.g., Alfvén waves) by non-isotropic particle distributions. Particle coupling to magnetic fields is particularly strong due to the high field strength in a SBN and its disordered morphology, affecting both particle energy distributions and transport properties. Under such conditions particle-field energy equipartition would be expected.

3. Particle and field energy densities

In repeated crossings of the shock region fast electrons and protons in the ambient SNR gas gain energy from their initial fiducial kinetic energy $T_0 \simeq 10$ keV (in the Maxwellian tail) to a very high value, $O(10^5)$ GeV. In the immediate vicinity of the acceleration sites, and before energy losses substantially modify their initial distributions, the particle spectral densities are usually assumed to have a power-law (in momentum p) form, $N_j(p) = N_{0,j} p^{-q_j}$ with $j = e, p$ for, respectively, electrons and protons; in general, $q_e \neq q_p$. If the ‘gas’ of nonthermal electrons and protons is approximated as an electrically neutral ‘plasma’, then

$$n_o = \int_{T_0}^{\infty} N_e(T) dT = \int_{T_0}^{\infty} N_p(T) dT. \quad (2)$$

The basic energy-momentum relation yields $dp/dT = (T/c^2 + m)(T^2/c^2 + 2Tm)^{-1/2}$, and using $N_j(T) = N_j[p(T)] dp/dT$, an explicit expression for $N_j(T)$ is obtained (e.g., Schlickeiser 2002)

$$N_j(T) = \frac{N_{0,j}}{c^2} (T + m_j c^2) \left(\frac{T^2}{c^2} + 2Tm_j \right)^{-(q_j+1)/2}. \quad (3)$$

The respective normalization can now be obtained by performing the integration in Eq.(2):

$$N_{0,j} = n_o (q_j - 1) \left[\frac{T_0^2}{c^2} + 2T_0 m_j \right]^{(q_j-1)/2}. \quad (4)$$

The p/e *number* density ratio, $\zeta = N_p(T)/N_e(T)$, can now be explicitly written

$$\begin{aligned} \zeta(T; q_p, q_e) &= \frac{(q_p - 1)}{(q_e - 1)} \frac{[T_0^2 + 2T_0 m_p c^2]^{\frac{q_p-1}{2}}}{[T_0^2 + 2T_0 m_e c^2]^{\frac{q_e-1}{2}}} \times \\ &\times \frac{T^{-\frac{(q_p+1)}{2}} (T + m_p c^2) (T + 2m_p c^2)^{-\frac{q_p+1}{2}}}{T^{-\frac{(q_e+1)}{2}} (T + m_e c^2) (T + 2m_e c^2)^{-\frac{q_e+1}{2}}}. \end{aligned} \quad (5)$$

When it is assumed that $q_p = q_e = q$, simpler limiting expressions for this ratio are obtained (e.g., Schlickeiser 2002)

$$\zeta(T; q) = \begin{cases} 1 & \dots T \ll m_e c^2 \\ \propto \left(\frac{T}{m_p c^2} \right)^{\frac{q-1}{2}} & \dots m_e c^2 \ll T \ll m_p c^2 \\ \left(\frac{m_p}{m_e} \right)^{\frac{q-1}{2}} & \dots T \gg m_p c^2. \end{cases} \quad (6)$$

The general expression for the p/e *energy* density ratio,

$$\kappa(T_0; q_p, q_e) = \frac{\int_{T_0}^{\infty} N_p(T) T dT}{\int_{T_0}^{\infty} N_e(T) T dT}, \quad (7)$$

can also be written down:

$$\begin{aligned} \kappa(T_0; q_p, q_e) &= \frac{(q_p - 1)}{(q_e - 1)} \frac{(T_0^2 + 2T_0 m_p c^2)^{\frac{q_p-1}{2}}}{(T_0^2 + 2T_0 m_e c^2)^{\frac{q_e-1}{2}}} \times \\ &\times \frac{\int_{T_0}^{\infty} T^{-\frac{q_p-1}{2}} (T + 2m_p c^2)^{-\frac{q_p+1}{2}} (T + m_p c^2) dT}{\int_{T_0}^{\infty} T^{-\frac{q_e-1}{2}} (T + 2m_e c^2)^{-\frac{q_e+1}{2}} (T + m_e c^2) dT}. \end{aligned} \quad (8)$$

In order to explore the relevant range of values of this ratio, we computed κ for several representative values of q_p and q_e (see Table 1). An approximate expression for κ can be obtained by considering only proton and electron energies higher than the respective particle mass,

$$\begin{aligned} \kappa(q_p, q_e) &\simeq \frac{(q_p - 1)}{(q_e - 1)} \frac{(q_e - 2)}{(q_p - 2)} \frac{(2T_0 m_p c^2)^{\frac{q_p-1}{2}}}{(2T_0 m_e c^2)^{\frac{q_e-1}{2}}} \times \\ &\times \frac{(m_p c^2)^{2-q_p}}{(m_e c^2)^{2-q_e}} \end{aligned} \quad (9)$$

which for $q_p = q_e = q$ reduces to

$$\kappa(q) \simeq \left(\frac{m_p}{m_e} \right)^{(3-q)/2}. \quad (10)$$

This expression for the energy density ratio (Eq. 10) is the analogous to the high-energy limit of the density ratio (Eq. 6).

To determine U_p from the theoretically predicted value of κ and U_e , which is deduced from the measured radio flux, obviously requires knowledge of the mean magnetic field in the emitting region, B . To overcome this (implied) indeterminacy, the assumption of field and particle energy equipartition is commonly made. Also, the contribution of secondary electrons (from π^- decay)² to the (steady state) electron density has to be included.

While the exact form of the particle steady-state spectral density does not generally have a single power-law form (e.g., Rephaeli 1979), the radiative yields are largely by protons and electrons with energies higher than a few GeV, for which Coulomb losses (which flatten the spectral density) are subdominant. In this limit, the total electron spectral density can be approximated by

$$N_e(\gamma) = N_{e,0} (1 + \chi) \gamma^{-q_e}, \quad (11)$$

where the electron Lorentz factor γ is in the range $\gamma_1 \leq \gamma \leq \gamma_2$, $N_{e,0}$ is a normalization factor of the primary electrons, and χ is the secondary-to-primary electron ratio. The electron spectral index is $q_e \geq 2$, with the minimal value of 2 corresponding to the strong-shock limit of the Fermi-I acceleration mechanism.

Ignoring the contribution of low-energy electrons with $\gamma < \gamma_1$, the electron energy density is $U_e \simeq N_{e,0} (1 + \chi) m_e c^2 \int_{\gamma_1}^{\gamma_2} \gamma^{1-q_e} d\gamma$, where γ_2 is the upper end of the electron energy spectrum. For $q_e > 2$,

$$U_e = N_{e,0} (1 + \chi) m_e c^2 \gamma_1^{2-q_e} \frac{[1 - (\gamma_2/\gamma_1)^{2-q_e}]}{(q_e - 2)}. \quad (12)$$

² Secondary positrons (from π^+ decay) almost immediately annihilate with thermal electrons.

Table 1. Proton-to-electron energy density ratios, κ ^[a].

q_p	q_e	κ	q_p	q_e	κ	q_p	q_e	κ	q_p	q_e	κ	q_p	q_e	κ
2.0	2.0	0.258E+02	2.1	2.0	0.984E+01	2.2	2.0	0.418E+01	2.3	2.0	0.197E+01	2.4	2.0	0.101E+01
2.0	2.1	0.628E+02	2.1	2.1	0.239E+02	2.2	2.1	0.102E+02	2.3	2.1	0.479E+01	2.4	2.1	0.246E+01
2.0	2.2	0.119E+03	2.1	2.2	0.453E+02	2.2	2.2	0.193E+02	2.3	2.2	0.906E+01	2.4	2.2	0.466E+01
2.0	2.3	0.189E+03	2.1	2.3	0.720E+02	2.2	2.3	0.306E+02	2.3	2.3	0.144E+02	2.4	2.3	0.740E+01
2.0	2.4	0.269E+03	2.1	2.4	0.102E+03	2.2	2.4	0.436E+02	2.3	2.4	0.205E+02	2.4	2.4	0.105E+02
2.0	2.5	0.357E+03	2.1	2.5	0.136E+03	2.2	2.5	0.578E+02	2.3	2.5	0.272E+02	2.4	2.5	0.140E+02
2.0	2.6	0.451E+03	2.1	2.6	0.172E+03	2.2	2.6	0.731E+02	2.3	2.6	0.344E+02	2.4	2.6	0.177E+02
2.0	2.7	0.551E+03	2.1	2.7	0.210E+03	2.2	2.7	0.892E+02	2.3	2.7	0.420E+02	2.4	2.7	0.216E+02
2.0	2.8	0.654E+03	2.1	2.8	0.249E+03	2.2	2.8	0.106E+03	2.3	2.8	0.499E+02	2.4	2.8	0.256E+02
2.0	2.9	0.760E+03	2.1	2.9	0.289E+03	2.2	2.9	0.123E+03	2.3	2.9	0.579E+02	2.4	2.9	0.298E+02
2.0	3.0	0.867E+03	2.1	3.0	0.330E+03	2.2	3.0	0.140E+03	2.3	3.0	0.661E+02	2.4	3.0	0.340E+02

^[a] An energy range of 10^{-5} GeV – 10^5 GeV is assumed.

For a population of electrons described by Eq.(11), traversing a homogeneous magnetic field of strength B that permeates a region with (a spherically equivalent) radius r_s located at a distance d , and emitting a 5 GHz synchrotron radiation flux of f_5 Jy, the standard synchrotron formula (e.g., Blumenthal & Gould 1970) yields

$$N_{e,0}(1 + \chi) = 1.6 \times 10^{-16} a_{q_e}^{-1} \psi_5 1250^{\frac{q_e}{2}} B^{-\frac{q_e+1}{2}} \quad (13)$$

where quantities are expressed in c.g.s. units, the factor a_{q_e} is defined and tabulated (in, e.g., Blumenthal & Gould 1970), and $\psi_5 \equiv (\frac{r_s}{0.1 \text{ kpc}})^{-3} (\frac{d}{\text{Mpc}})^2 (\frac{f_5}{\text{Jy}})$. From Eqs.(12, 13) we derive

$$U_e = 1.3 \times 10^{-22} 1250^{\frac{q_e}{2}} \psi_5 B^{-\frac{q_e+1}{2}} \times \frac{\gamma_1^{2-q_e} [1 - (\gamma_2/\gamma_1)^{2-q_e}]}{(q_e - 2) a_{q_e}} \text{ erg cm}^{-3}. \quad (14)$$

Since U_e includes both primary and secondary electrons, the rough assumption that both populations can be characterized with nearly the same power law index³ means that the primary electron energy is $U_e/(1 + \chi)$. Denoting the primary p/e energy density ratio (see Sect. 3) by $\kappa(q_p, q_e)$, the proton

energy density is

$$U_p \simeq \kappa(q_p, q_e) \frac{U_e}{1 + \chi}. \quad (15)$$

Since tight coupling is expected in the very dense environment of SBN, particle and magnetic field energy densities can be assumed to be close to equipartition (see Eq.(21). If so, we can express the field in terms of the total particle energy density; this leads to

$$U_p = \frac{2.5 \times 10^{10}}{1 + (1 + \chi)/\kappa} \left[3.3 \times 10^{-21} \left(1 + \frac{\kappa}{1 + \chi} \right) \gamma_1^{2-q_e} \times \frac{[1 - (\gamma_2/\gamma_1)^{2-q_e}] 1250^{q_e/2} \psi_5}{(q_e - 2) a_{q_e}} \right]^{4/(5+q_e)} \text{ eV cm}^{-3}. \quad (16)$$

In general, q_e , q_p , χ , γ_1 , γ_2 , and κ need to be known (or assumed) in order to compute U_p . The value of q_e is readily deduced from measurements of the (nonthermal) radio spectral index, α , through the relation $q_e = 2\alpha + 1$.

3.1. Proton spectral index

The proton spectral index has been measured in the nearby SBGs NGC 253, NGC 3034, NGC 4945 (Ackermann et al. 2012), $q_p \simeq 2.2$. As we discuss below, it can be expected that this value characterizes proton spectra also in other SBGs.

Suprathermal particles injected into a supernova shock have a power law spectrum with index $q = (R + 2)/(R - 1)$, where R is the shock compression ratio, defined as the downstream to upstream density, ρ_d/ρ_u . In an ideal gas, $R = (\gamma + 1)/[(\gamma - 1) + 2/M_u^2]$, where γ is the ratio of the gas specific heats, $M_u = v_u/c_s$ is the shock Mach number, and c_s is the sound speed. Since $c_s = \sqrt{\gamma p_u/\rho_u}$, clearly $M_u = v_u/\sqrt{\gamma k_B T_u/(\mu m_p)}$. The temperature of the upstream medium, T_u , is nearly two orders of magnitude higher ($T \sim 10^{6-7}$ °K) in SB regions than in more quiescent galactic disks ($T \sim 10^{4-5}$ °K) (Heckman & Lehnert 2000; Fujita et al. 2009). Therefore for a given shock velocity v_u , during the Sedov phase of SNR the Mach number is smaller in the SBN than in the disk, so that the compression ratio of a strong shock in the SBN is expected to be $R \simeq 3.6$,

³ Theoretical expectation is that power-law indices of proton and electron source spectra are nearly identical. Under typical inter-stellar conditions, electrons lose energy more efficiently than protons, resulting in a relative steepening of the electron spectrum. Secondary electrons (and positrons, produced in π^\pm decays following pp collisions) initially have a slightly flatter spectrum (by $\Delta q \simeq 0.2$) than the parent proton spectrum for energies $\gtrsim 1$ GeV, but then their spectrum steepens due to severe energy losses. Detailed numerical models of emission from starburst galaxies show that primary and secondary electrons have roughly similar spectral shapes at energies ~ 10 MeV – 1 TeV (e.g., Domingo-Santamaría & Torres 2005; De Cea del Pozo et al. 2009; Rephaeli et al. 2010). Therefore, in the relatively small SBN region, where energetic particles have not yet ventured out too far from are their acceleration sites, it is quite reasonable (for our purposes here) to characterize their spectra with the same index. After all, from a practical point of view, both primary and secondary electrons contribute to the main observable upon which we base our analysis - radio emission - which is described by a single-index power-law spectrum.

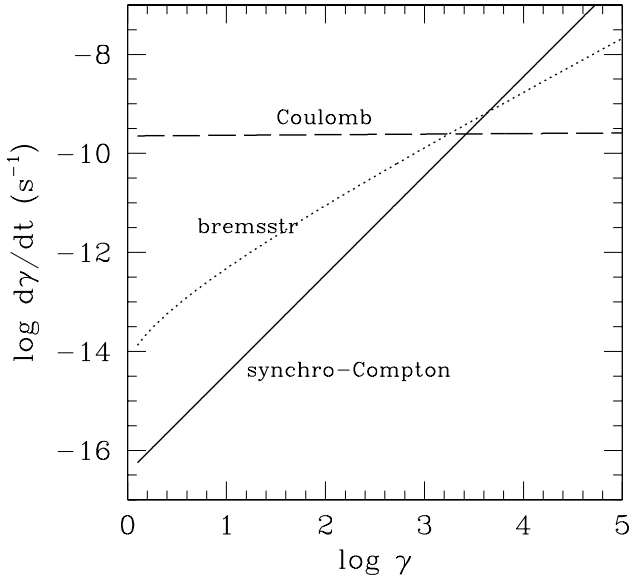


Fig. 1. Energy loss rates of an electron of energy $\gamma m_e c^2$ due to Coulomb, bremsstrahlung, and synchrotron-Compton processes in a typical (M 82-like) SBN environment: $B = 100 \mu\text{G}$, $L_{\text{IR}} = 10^{44} \text{ erg s}^{-1}$, $r_s = 0.2 \text{ kpc}$, $n = 100 \text{ cm}^{-3}$, $n_e = 200 \text{ cm}^{-3}$.

somewhat lower than the more typical (Galactic) value $R \simeq 4$. This lower value implies an injection index in the range $2.0 \leq q \leq 2.3$ (Fujita et al. 2009).

3.2. Electron secondary-to-primary ratio

The secondary-to-primary electron ratio χ depends on the injection p/e number ratio, ζ , and on the gas density, which determines the effectiveness of proton-proton (pp) interactions that yield charged and neutral pions. An electron is produced in the decay $\pi^- \rightarrow \mu^- + \bar{\nu}_\mu$, followed by $\mu^- \rightarrow e^- + \bar{\nu}_e + \nu_\mu$; a positron is produced in the decay $\pi^+ \rightarrow \mu^+ + \nu_\mu$, followed by $\mu^+ \rightarrow e^+ + \nu_e + \bar{\nu}_\mu$. The pp branching ratios are such that in 2/3 of these interactions e^\pm are produced.

The mean free path of an energetic proton for pp interactions in a gas with density n is $\lambda_{pp} = (\sigma_{pp} n)^{-1}$. The pp cross section for protons with kinetic energy of a few TeV is $\sigma_{pp} \approx 50 \text{ mb} = 5 \times 10^{-26} \text{ cm}^2$ (Baltrusaitis et al. 1984), so that the probability for a proton to undergo pp interactions during its 3D random walk through a region of radius r_s is then $\sqrt{3} r_s / \lambda_{pp}$. Given the injection p/e ratio, ζ , and the above branching ratio, the secondary-to-primary electron ratio is

$$\chi = \frac{2}{3} \zeta \sqrt{3} r_s n \sigma_{pp}. \quad (17)$$

In a typical SBN with $r_s = 0.2 \text{ kpc}$, $n = 200 \text{ cm}^{-3}$, and $q = 2.2 - 2.3$, estimated values of χ are $\sim 0.6 - 1$, in accord with results from more detailed numerical models (e.g., Paglionie et al. 1996; Domingo-Santamaría & Torres 2005; De Cea et al. 2009; Rephaeli et al. 2010).

3.3. Equipartition magnetic field

As we have already noted, it is quite likely that in their equilibrium minimum-energy configuration particles and magnetic fields, which are tightly coupled dynamically and energetically in the SN environment, are in energy equipartition. We assume that equipartition is indeed attained during the SB phase, and use it to determine the mean magnetic field in the SBN region. The starting point is an estimate of the electron energy density from the measured radio flux. To do so we integrate the electron spectral energy density over the interval $[\gamma_1, \gamma_2]$.

For consistency with the assumed power-law form of the electron spectral density, we take the low-energy limit γ_1 to be the value of the Lorentz factor at which the sum of the Coulomb (or electronic excitation, in ionized gas) and bremsstrahlung loss rates equals the synchrotron-Compton loss rate. This is based also on the fact that even for the relatively high values of the magnetic field in SBN, the measured radio emission (upon which our normalization of the electron density is based) samples electrons with $\gamma > 10^3$.

The Coulomb (electronic excitation) loss rate (e.g., Rephaeli 1979) is

$$b_0 = -\dot{\gamma}_c \simeq 1.2 \times 10^{-12} n_e \left[1.0 + \frac{\ln(\gamma/n_e)}{84} \right] \text{ s}^{-1} \quad (18)$$

where n_e is the (thermal) electron number density.

The closely related bremsstrahlung loss rate for a H+He plasma with solar abundances, that also includes the contribution of e-e scatterings, is (Gould 1975)

$$b_1 = -\dot{\gamma}_b \simeq \begin{cases} 1.78 \times 10^{-16} n \gamma [\ln(\gamma) + 0.36] \text{ s}^{-1} & \text{ion} \\ 9.44 \times 10^{-16} n \gamma \text{ s}^{-1} & \text{neutr} \end{cases} \quad (19)$$

where n denotes the number density of hydrogen nuclei. The reported expression for neutral plasma holds for $\gamma \geq 100$, at lower γ the ionized and neutral cases essentially overlap (Gould 1975).

The higher order (in γ) synchrotron-Compton loss rate (e.g., Blumenthal & Gould 1970) is

$$b_2 = -\dot{\gamma}_{\text{SC}} = 1.3 \times 10^{-9} \gamma^2 (B^2 + 8\pi \rho_{\text{IR}}) \text{ s}^{-1}, \quad (20)$$

where ρ_{IR} is the energy density of the (dominant) IR radiation field in the SBN region.

Equating the sum of the first two loss rates with the latter yields an estimate of γ_1 . In Fig. 1 we display the energy-loss rates, expressed in Eqs.(18)-(20), for typical SBN parameters. In our numerical estimates (see Table 2) we use the second of Eqs.(19) for the mostly-neutral SBNs in Arp 220 and Arp 299-A, and the first for the other, mostly-ionized SBNs.

Whereas the dependence of the electron energy density on γ_1 is appreciable, since $\gamma_2 > 10^5$ the exact value of the upper end of the γ integral is of little significance for the range of values of q_e of interest here; in our calculations we take $\gamma_2 = 10^5$.

With both U_e and U_p determined, the mean field strength is deduced from

$$\frac{B^2}{8\pi} = \eta (U_p + U_e) \quad (21)$$

where $\eta = 1$ in equipartition, but somewhat lower, $\eta = 3/4$, in strictly minimum-energy configuration (Longair 1981)⁴. In terms of the particle p/e energy density ratio, κ , the particle-field coupling condition is $B^2/8\pi = \eta U_p [1 + (1 + \chi)/\kappa]$, so that

$$B = \sqrt{\eta} \left[3.3 \times 10^{-21} \left(1 + \frac{\kappa}{1 + \chi} \right) 1250^{q_e/2} \psi_5 \times \right. \\ \left. \times \gamma_1^{2-q_e} \frac{[1 - (\gamma_2/\gamma_1)^{2-q_e}]^{2/(5+q_e)}}{(q_e - 2) a_{q_e}} \right] G \quad (22)$$

Given the values of n , the size of the SBN region, and the IR energy density (which is computed from the L_{IR} and the region size), as listed in Table 2, the expression for B in the last equation (with $\eta = 1$) can be inserted in Eq.(20), and using the other two loss rate equations, the value of γ_1 can be deduced. This value of γ_1 is then substituted in the equation for B to obtain the equipartition value of the mean field. We note that in most cases the corresponding synchrotron frequency, $\nu_1 = 4B\gamma_1^2$ MHz, where the radio spectrum is expected to curve to a flatter slope for decreasing frequencies, is comparable to our reference frequency of 5 GHz.

4. Proton energy densities in SBNs

In SB galaxies star formation is very intense in a relatively small nuclear region (the SBN) with effective radius $r_s \approx 0.2$ kpc – with $r_s \equiv (3/4 R_{\text{sb}}^2 h_{\text{sb}})^{1/3}$, where R_{sb} and h_{sb} are the radius and height of the region. By contrast, low-intensity star formation quiescently proceeds throughout the galactic disk (as in normal, i.e., non-SB, spirals, such as the Galaxy).

For a sample of local SBN, values of U_p and B were calculated using the relevant observational quantities in Table 2, starting with the radio flux and spectral index. Due to the appreciable observational uncertainties – mostly in the value of the gas density, the size of the emitting region, and modeling uncertainties – the derived values of B and U_p are also uncertain, typically by a factor which we estimate to be ~ 1.4 and ~ 2 . While our results for these two quantities would not seem to be that precise, it should be emphasized that some of the uncertainties are inherent given the basic difficulties in determining the size of the SBN region, the measurement of the gas density in this region, limited spatial resolution, and the rudimentary level of the spectral γ -ray measurements. Note that in light of these substantial uncertainties the (modeling) uncertainty in the

value of the mean magnetic field when calculated assuming energy equipartition as compared to minimum energy configuration is relatively insignificant. For example, for the two nearby SBG, NGC 253 and NGC 3034, values of B are only $\sim 15\%$ lower in the minimum energy configuration as compared to the equipartition values (listed in Table 2).

Our electron-based estimates of the proton energy densities are in agreement with γ -ray measurements of π^0 -decay emission for the three galaxies NGC 253, NGC 3034 (M 82), and NGC 4945 for which such emission was detected. The results for the very compact SBNs of Arp 220 and Arp 299-A represent extreme cases: small source regions and relatively hard electron spectra result in high magnetic fields and high CR energy densities, $B \sim 0.2$ mG and $U_p \sim 500$ eV cm⁻³. However, it is questionable whether in such extreme environments, with conditions that are more typical of SN remnants, steady-state and equipartition are actually attained (e.g., Torres 2004). The unusually high values of γ_1 derived for these highly compact nuclei may signal, in fact, a breakdown in our assumptions – the most critical one being particle-field equipartition.

5. Discussion

Active star formation leads to particle acceleration by SN shocks. Considerations of the acceleration, relevant energy losses, and SB timescales, indicate that relativistic proton and electron distributions reach steady-state during most of the SB phase. And given the tight coupling between the particles and magnetic fields in the dense plasma, it is quite likely that energy equipartition is achieved in the SBN region. With an assumed theoretically motivated p/e ratio, the assumption of equipartition provides the requisite relation to determine particle energy densities and the mean field from spectral radio measurements.

Essential to this radio-based method is a reliable estimate of the p/e energy ratio, κ . Adopting the common assumption of an overall electrically neutral nonthermal ‘plasma’, we derived an approximate expression for this ratio as a function of the electron and proton spectral indices, q_e and q_p . We note that, in the limit of $q_e = q_p = q$ (e.g., at injection), $\kappa \simeq (m_p/m_e)^{(3-q)/2}$; this simple relation is supplementary to the analogous, well-known p/e number ratio, $N_p/N_e = (m_p/m_e)^{(q-1)/2}$ (e.g., Schlickeiser 2002). Even though the assumptions of single-index steady-state spectra and particle-field equipartition may be unrealistic, at our present knowledge of the SBN environment relaxing any of these simplifications necessarily leads to a more parameter-rich formalism that will invariably result in arbitrariness in guessing parameter values in what is essentially an underdetermined problem.

For the determination of q_p , we have assumed that SBN spectra (in the observed *Fermi*/LAT and IACT energy ranges) are dominated by emission from π -decay – owing to the much higher star formation rate and mean (target) gas density in SBN than in the (rest of the) disk. The theoretical expectation of proton injection index in the range $2.0 \leq q \leq 2.3$ is fully consistent with the measured value $q_p \simeq 2.2$. Due to the lack of spatial information on the distribution of γ -ray emission in the nearby starburst galaxies, our expectation on the respective contributions of the SBN and disk regions is based on theoret-

⁴ Energy equipartition may be attained (over time) under conditions of tight coupling of the main matter and energy components of a physical environment in its minimum energy configuration. The electromagnetic emission of a SBN that directly comes from relativistic particles manifests itself in the radio and in γ -rays. The total energy density in the SBN responsible for such non-thermal emission is $U = U_{\text{CR}} + U_{\text{B}}$. As noted in Sect. 2, under physical conditions prevailing in a SBN the particles and the B-field behave like relativistic fluids tightly coupled with each other. Their equilibrium configuration most likely corresponds to a state of minimum energy, which is achieved for $U_{\text{B}} = \eta U_{\text{CR}}$ with $\eta = 3/4$ (Longair 1981). Clearly, this minimum-energy condition is very close to equipartition ($\eta = 1$), so at equilibrium the particle energy density nearly equals the field energy density.

Table 2. Starburst galaxies: data and results for high-energy activity.

Object	$D_L^{[1]}$	$R_{SB}^{[2]}$	$h_{SB}^{[3]}$	$f_5^{[4]}$	$\alpha^{[5]}$	$n_e^{[6]}$	$L_{IR}^{[7]}$	$M_{SB}^{[8]}$	$\chi^{[11]}$	$\kappa^{[12]}$	$\gamma_1^{[13]}$	$B^{[14]}$	$U_p^{[15]}$	Notes ^[a]
Arp 220 E	74.7	114 ⁺	–	0.08	0.70	3000 ⁺	44.91	9.3	24	48	21000	155	390	
Arp 220 W	74.7	70 ⁺	–	0.10	0.70	3000 ⁺	45.08	9.1	40	48	15000	230	730	
Arp 299-A	43.0	140	200*	0.10	0.60	250	44.88	9.0	8	20	8700	145	365	= IC 694
NGC 253	2.5	180	150	1.80	0.70	100	43.62	7.7	0.3	48	8300	100	235	
NGC 3034	3.4	300	200	3.70	0.71	200	43.96	8.1	0.3	51	6600	100	250	= M 82
NGC 3628	7.6	135	200*	.065	0.86	100	43.30	7.3	0.1	120	7600	65	100	
NGC 4945	3.7	250	200*	2.25	0.60	300	43.72	7.4	0.1	20	4700	110	270	
NGC 5236	3.7	180	200*	0.75	0.80	200	43.45	7.3	0.1	90	5000	105	260	= M 83
NGC 6946	5.5	150	200*	.045	0.74	100	43.51	7.0	0.7	60	4000	65	110	

^[1]Distance, in Mpc (from Ackermann et al. 2012).

^[2,3]Radius and height of (cylindrical) star-forming region, in pc (*: assumed; +: spherical). Data are from Torres 2004 and references therein (Arp 220), Sugai et al. 1999 (Arp 299-A), Carral et al. 1994 (NGC 253), Völk et al. 1996 (NGC 3034), Israel et al. 1990 (NGC 3628), Brock et al. 1988 (NGC 4945), Calzetti et al. 1999 (NGC 5236), Schinnerer et al. 2006 (NGC 6946).

^[4,5]Non-thermal 5 GHz flux density, in Jy, and spectral radio index. Data are from Torres 2004 (Arp 220), Bondi et al. 2012 (Arp 299-A), Rephaeli et al. 2010 and references therein (NGC 253), Klein et al. 1988 and Carlstrom & Kronberg 1991 (NGC 3034), Condon et al. 1982 (NGC 3628), Elmouttie et al. 1997 (NGC 4945), Sukumar et al. 1987 (NGC 5236), Murphy et al. 2011 (NGC 6946).

^[6]Thermal electron density, in cm^{-3} (*: assumed). Data are taken or computed from Yun et al. 2004 (Arp 220), Sugai et al. 1999 and Zhao et al. 1997 (Arp 299-A), Engelbracht et al. 1998 (NGC 253), Petuchowski et al. 1994 (NGC 3034), Dahlem et al. 1996 (NGC 3628), Lipari et al. 1997 and Spoon et al. 2000 (NGC 4945), Krabbe et al. 2014 (NGC 5236), Engelbracht et al. 1996 (NGC 6946).

^[7]Log of the total IR (8–1000 μm) luminosity (erg s^{-1} ; Ackermann et al. 2012, and Charmandaris et al. 2002 for Arp 299-A).

^[8]Log of ISM mass in the SB (in M_\odot). Data are from Torres 2004 (Arp 220), Charmandaris et al. 2002 (Arp 299-A), Carral et al. 1994 and Domingo-Santamaría & Torres 2005 (NGC 253), Rickard et al. 1977, Rieke et al. 1980, Weiss et al. 2001 (NGC 3034), Israel et al. 1990 (NGC 3628), Spoon et al. 2000 (NGC 4945), Israel & Baas 2001 (NGC 5236, NGC 6946).

^[9]CRp spectral index.

^[10]Secondary-to-primary electron ratio.

^[11]p/e energy density ratio.

^[12]Electron Lorentz factor at which Coulomb and synchrotron energy losses are equal.

^[13]Equipartition magnetic field, in μG .

^[14]Equipartition CR proton energy density, in eV cm^{-3} .

^[a]Arp 220 E and W denote, respectively, the East and West extreme starbursts embedded in Arp 220’s molecular disk (see Torres 2004 and references therein). NGC 4945 hosts a Seyfert-1 nucleus but its HE emission is dominated by the SBN (Spoon et al. 2000; Lenain et al. 2010).

ical predictions, particularly our own detailed numerical modeling of the emission in M 82 and NGC 253 (using a modified version of the GALPROP code: Persic et al. 2008 and Rephaeli et al. 2010; see also Domingo-Santamaría & Torres 2005 for NGC 253). These analyses do suggest that while the relative contribution of the disk is not negligible, it comprises only a small fraction due to further steepening of the particle spectra in the disk. However, given the uncertainty in the exact values of both the measured and predicted power-law indices, there is also an uncertainty in the relative contributions of the SBN and disk.

Our work here improves on our earlier discussion and partial implementation of the radio-based method for determining electron and proton energy densities in active regions of star formation (Persic & Rephaeli 2010). We do so by accounting for electron radiative losses, by using a more accurate calculation of the p/e ratio, and basing our approach on insight gained from our previous implementation of a modified version of the GALPROP code that fully accounts for both spectral and spatial evolution of proton and electron distributions in the SB region and throughout the disk (Persic et al. 2008; Rephaeli et al. 2010). Our general approach and its quantitative imple-

mentations for predicting the high-energy spectra of the SBGs NGC 253 and NGC 3034 have been validated by good agreement with γ -ray measurements (Acero et al. 2009; Acciari et al. 2009; Ackermann et al. 2012).

Following on previous work (Beck & Krause 2005), in a recent paper Lacki & Beck (2013, hereafter LB13) discussed the validity of field-particles equipartition in a SB environment, accounting for secondary electrons and strong energy losses. While their main conclusions on deducing U_p from radio measurements do agree with ours (in both Persic & Rephaeli 2010, and in this work), there are substantial differences between our respective treatments. First, we start with the electron spectrum as deduced from radio measurements, including the contribution of secondary electrons to the emission. We then use an analytically derived primary p/e energy density ratio (using the relevant parameter values) to compute U_p . In contrast, the starting point of the LB13 analysis is the proton energy density, which they take to be related to the electron energy density by the same factor, 75, for all the galaxies in their sample. Second, whereas we assume electric neutrality of the accelerated particles to determine the primary p/e ratios for different electron and proton spectral indices, LB13 start from an as-

sumed universal p/e number density ratio, which they adjust by accounting for the electrons energy losses. Third, we compute the secondary-to-primary electron number ratio by using the primary p/e number ratio, the mean proton free path in a gas with a given density, and the branching ratios in pp interactions, whereas LB13 estimate this ratio by scaling the injection p/e ratio by 1/6 times the value of the estimated fraction of the proton energy that goes into π^\pm . These differences in approach and implementation led to substantially different results for U_p and B (listed in our Table 2 and their Table 3). Whatever the details, it should be remarked that for the nearby starburst galaxies NGC 253, NGC 3034, and NGC 4945 our estimated U_p and B agree with results of direct measurements. This agreement suggests that the equipartition assumption we made to derive CR and B energy densities is globally verified in these SBNs – at least as an average property. For NGC 3034 this suggestion was made early on by Völk et al. (1990) on the condition that $\zeta(> 1 \text{ GeV}) \sim 10^2$ – condition that is consistent with our procedure, see Eq.6.

If the agreement between radio estimates and γ -ray measurements of U_p and B in SBNs is further validated and established, the radio method for reliable estimation of proton energy densities will be particularly useful for distant ($z \gtrsim 1$) galaxies, whose intense star formation is exemplified (albeit at lower levels) by the nearby SBGs, but whose faint γ -ray fluxes are not detectable with current or upcoming instruments whereas their $< 0.1 \text{ mJy}$ radio fluxes are (e.g., Tozzi et al. 2009).

References

- Acciari, V.A., et al. (VERITAS Collab.) 2009, *Nature*, 462, 770
- Acero, F., et al. (HESS Collab.) 2009 *Science*, 326, 1080
- Ackermann, M., et al. (LAT Collab.) 2012, *ApJ*, 755, A164
- Baltrusaitis, R.M., et al. 1984, *PRL*, 52, 1380
- Beck, R., & Krause, M., 2005, *Astr. Nacht.*, 326, 414
- Blumenthal, G.R., & Gould, R.J. 1970, *Rev. Mod. Phys.*, 42, 237
- Bondi, M., Perez-Torres, M.A., Herrero-Illana, R., & Alberdi, A. 2012, *ApJ*, 539, A134
- Brock, D., Joy, M., Lester, D.F., Harvey, P.M. & Ellis, H.B., Jr. 1988, *ApJ*, 329, 208
- Calzetti, D., Conselice, Ch.J., Gallagher, J.S., & Kinney, A.L. 1999, *AJ*, 118, 797
- Carlstrom, J.E., & Kronberg, Ph.P. 1991, *ApJ*, 366, 422
- Carral, P., Hollenbach, D.J., Lord, S.D., et al. 1994, *ApJ*, 423, 223
- Charmandaris, V., Stacey, G.J., & Gull, G. 2002, *ApJ*, 571, 282
- Chevalier, R.A., & Clegg, A.W. 1985, *Nature*, 317, 44
- Condon, J.J., Condon, M.A., Gisler, G., & Puschell, J.J. 1982, *ApJ*, 252, 102
- Dahlem, M., Heckman, T.M., Fabbiano, G., Lehnert, M.D., & Gilmore, D. 1996, *ApJ*, 461, 724
- de Cea Del Pozo, E., Torres, D.F., & Rodriguez Marrero, A.Y., 2009, *ApJ*, 698, 1054
- Domingo-Santamaría, E., & Torres, D.F., 2005, *A&A*, 444, 403
- Drury, L.O'C., Aharonian, F.A., & Völk, H.J. 1994, *A&A*, 287, 959
- Elmouttie M., Haynes R.F., Jones, K.L., et al. 1997, *MNRAS*, 284, 830
- Engelbracht, C.W., Rieke, M.J., Rieke, G.H., & Latter, W.B. 1996, *ApJ*, 467, 227
- Engelbracht, C.W., Rieke, M.J., Rieke, G.H., Kelly, D.M. & Achtermann, J.M. 1998, *ApJ*, 505, 639
- Fujita, Y., Ohira, Y., Tanaka, S.J., & Takahara, F. 2009, *ApJ*, 707, L179
- Gaisser, T.K. 1990, *Cosmic Rays and Particle Physics* (Cambridge: Cambridge University Press)
- Gould, R.J. 1975, *ApJ*, 196, 689
- Heckman, T.M., & Lehnert, M.D. 2000, *ApJ*, 537, 690
- Krabbe, A.C., Rosa, D.A., Dors O.L., Jr., et al. 2014, *MNRAS*, 437, 1155
- Klein U., Wielebinski R., & Morsi, H.W. 1988, *A&A*, 190, 41
- Israel, F.P., Baas, F., & Maloney, P.R. 1990, *A&A*, 237, 17
- Israel, F.P., & Baas, F. 2001, *A&A*, 371, 433
- Lacki, B.C., & Beck, R. 2013, *MNRAS*, 430, 3171
- Lenain J.-P., Ricci C., Türler M., Dorner D., & Walter R. 2010, *A&A*, 524, 72L
- Lipari, S., Tsvetanov Z., & Macchetto F. 1997, *ApJSS*, 111, 369
- Longair M.S., 1981, *High Energy Astrophysics* (1st ed.; Cambridge: Cambridge Univ. Press)
- Murphy, E.J., Condon, J.J., Schinnerer, E., et al. 2011, *ApJ*, 737, 67
- Paglione, T.A.D., Marscher, A.P., Jackson, J.M., & Bertsch D.L., 1996, *ApJ*, 460, 295
- Persic, M., & Rephaeli, Y. 2010, *MNRAS*, 403, 1569
- Persic, M., Rephaeli, Y., & Arieli, Y. 2008, *A&A*, 486, 143
- Petuchowski, S.J., Bennett, C.L., Haas, M.R., et al. 1994, *ApJ*, 427, L17
- Rephaeli, Y. 1979, *ApJ*, 227, 364
- Rephaeli, Y., Arieli, Y., & Persic, M. 2010, *MNRAS*, 401, 473
- Rickard, L.J., Palmer, P., Morris, M., Turner, B.E., & Zuckerman, B. 1977, *ApJ*, 213, 673
- Rieke, G.H., Lebofsky, M.J., Thompson, R.I., Low, F.J., & Tokunaga, A.T. 1980, *ApJ*, 238, 24
- Schinnerer, E., Böker, T., Emsellen, E., & Lisenfeld, U. 2006, *ApJ*, 649, 181
- Schlickeiser R., 2002, *Cosmic Ray Astrophysics* (Berlin: Springer), p.472
- Spoon, H.W.W., Koornneef, J., Moorwood, A.F.M., Lutz, D., & Tielens, A.G.G.M. 2000, *A&A*, 357, 898
- Strickland, D.K., & Heckman, T.M., 2009, *ApJ*, 697, 2030
- Sugai, H., Davies, R.I., Malkan, M.A., et al. 1999, *ApJ*, 527, 778
- Sukumar, S., Klein, U., & Gräve, R. 1987, *A&A*, 184, 71
- Torres, D.F., 2004, *ApJ*, 617, 966
- Tozzi, P., Mainieri, V., Rosati, P., et al. 2009, *ApJ*, 698, 740
- Völk, H.J., Aharonian, F.A. & Breitschwerdt, D., 1996 *Space Science Rev.* 75, 279
- Völk, H.J., Klein, U., & Wielebinski, R. 1990, *A&A*, 237, 21
- Weiss, A., Neininger, N., Hüttemeister, S., & Klein, U. 2001, *A&A*, 365, 571
- Yun, M.S., Scoville, N.Z., & Shukla, H. 2004, in "The Neutral ISM in Starburst Galaxies", ASP Conference Series Vol.320 (eds. S Aalto, S. Hüttemeister, & A. Pedlar), 27
- Zhao, J.-H., Anantharamaiah, K.R., Goss, W.M., & Viallefond, F. 1997, *ApJ*, 482, 186